Additive Manufacturing 36 (2020) 101398

Contents lists available at ScienceDirect

Additive Manufacturing

journal homepage: www.elsevier.com/locate/addma

Fatigue behavior of additively manufactured 17-4 PH stainless steel: The effects of part location and powder re-use

Arash Soltani-Tehrani[a,b], Jonathan Pegues[a,b], Nima Shamsaei[a,b,*]

[a] National Center for Additive Manufacturing Excellence (NCAME), Auburn University, Auburn, AL, 36849, USA
[b] Department of Mechanical Engineering, Auburn University, Auburn, AL, 36849, USA

ARTICLE INFO

Keywords:
Fatigue
Laser beam powder bed fusion (LB-PBF)
Defects
Powder recycling
Part location

ABSTRACT

In laser beam powder bed fusion (LB-PBF), an additive manufacturing method, powder is often reconditioned and re-used multiple times to save cost. Considering the assumption that powder characteristics may affect the LB-PBF part quality, it is essential to understand how such characteristics change by re-using the powder and how these changes affect the mechanical properties of the fabricated part. Therefore, this study systematically investigates the effect of powder re-use on the powder characteristics, microstructural features, and mechanical properties of LB-PBF 17−4 precipitation hardening (PH) stainless steel (SS) specimens in both as-built and machined surface conditions. In addition, the dependency of microstructural features and mechanical properties on the location of the specimen on the build plate and how the powder re-use affects such location dependencies are studied. No significant effect of powder re-use and location dependency was observed on tensile or fatigue behavior of LB-PBF specimens in the as-built surface condition. However, an improved fatigue resistance, specifically in the high cycle regime, was observed for machined specimens fabricated by heavily re-used powder. In addition, considerable location dependency on the fatigue behavior was observed for machined specimens fabricated by unused powder. This location dependency, however, decreased with increasing powder re-use. The observed dependency of the fatigue behavior to the location and the improved fatigue resistance are explained by the better flowability and less compressibility of the re-used powder due to the decreased number of very fine particles and agglomerates within the powder batch. These improved powder characteristics resulted in a more uniform powder distribution on the build plate and less and smaller defects in the specimens.

1. Introduction

Additive manufacturing (AM) is an advanced manufacturing technology, which provides the opportunity to fabricate complex components directly from a 3D CAD model and material feedstock (i.e., powder or wire) in a layer by layer process. Powder is used as the feedstock in powder bed fusion (PBF) techniques, which are one of the most widely used AM methods [1]. One of the major challenges associated with powder feedstock, however, is the handling of previously used and recovered feedstock. A significant portion of the powder bed envelope is unfused after part fabrication and, for economic reasons, is often sieved and re-used for several iterations before being discarded. Currently, the effect of powder re-use on the resulting fatigue behavior of parts fabricated with increasingly re-used powder is not well understood. A common procedure to re-use metal powder is to collect all the powder in the collector bin and unconsolidated powder in the build envelope after fabrication, pass the collected powder through a sieve screen to remove large spatter particles and break down any agglomerates (i.e., clusters of small particles adhered to larger particles [1]), and mix to uniformity with an appropriate amount of additional powder to perform the next build.

While re-using the powder is a common practice, there are limited studies on how re-using the powder can alter the powder characteristics, and consequently, the mechanical performance of the fabricated part [1]. Some studies have been conducted in an effort to understand the effects of powder re-use on powder characteristics [2–8]. Effects of powder re-use on Ti-6Al-4V and Inconel 718 using electron beam powder bed fusion (EB-PBF) process were studied in [6], and no

Abbreviations: LB-PBF, laser beam powder bed fusion; PH, precipitation hardening; SS, stainless steel; AM, additive manufacturing, additive manufactured; PBF, powder bed fusion; EB-PBF, electron beam powder bed fusion; PSD, particle size distribution; UTS, ultimate tensile strength; YS, yield strength; HCF, high cycle fatigue; MCF, mid cycle fatigue; LCF, low cycle fatigue; B, Batch; CE, circular equivalent; SEM, scanning electron microscopy; LoF, Lack of fusion

* Corresponding author at: National Center for Additive Manufacturing Excellence (NCAME), Auburn University, Auburn, AL, 36849, USA.
E-mail address: shamsaei@auburn.edu (N. Shamsaei).

https://doi.org/10.1016/j.addma.2020.101398
Received 20 February 2020; Received in revised form 15 May 2020; Accepted 15 June 2020
Available online 22 June 2020

Nomenclature

A_0	initial cross-sectional area of the gauge
A_f	fracture cross-sectional area of the gauge
$2N_f$	number of reversals to failure
$E^{'}$	cyclic modulus of elasticity of the stable cycle
R_ε	ratio of minimum strain to the maximum strain
R_a	average surface roughness
ε_a	strain amplitude
ε_f	true fracture strain
σ_a	stress amplitude
σ_m	mean stress

significant changes in flowability, morphology, and particle size distribution (PSD) with re-using for five and six times, respectively for Ti-6Al-4V and Inconel 718, were observed. It was, however, found that the number of possible re-using times for Ti-6Al-4V can be limited to the amount of oxygen concentration due to its increase with powder re-use [6].

Cordova et al. [4] also studied the effects of re-using LB-PBF Inconel 718, Ti-6Al-4V, AlSi10Mg, and Scalmalloy on powder characteristics including morphology, flowability, microstructure, and chemical composition. Finer particles were reported to get eliminated with re-using the powder, leading to larger average particle sizes which was more drastic for AlSi10Mg. Some changes in morphology such as particles becoming more elongated were observed in the re-used Inconel 718 and AlSi10Mg. In addition, a general increasing trend of flowability was noticed for re-used powder as compared to unused powder for all the materials. While in these studies different powder features (including PSD, particle shape, chemistry and flowability) were characterized [2–8], the effects of powder re-using on the mechanical properties were not investigated.

Some studies have been recently conducted to understand the effects of powder re-use on the mechanical properties of the fabricated parts [9–18]. For instance, Popov et al. [17] observed shorter fatigue lives for specimens fabricated from EB-PBF 69-times re-used Ti-6Al-4V powder compared with the ones from unused powder. The shorter fatigue lives for the EB-PBF parts fabricated from re-used Ti-6Al-4V powder were explained by the particles' surface oxidation which led to lack of fusion defects in parts. While no changes in the microstructure of the fabricated parts were reported, a decrease in ductility of specimens fabricated by re-used powder was observed. In another study, the effects of re-used nickel alloy powder in LB-PBF on tensile properties were investigated [11]. Oxygen content increased with re-using the powder in LB-PBF. The increase in oxygen level resulted in lower ductility and toughness of the LB-PBF parts fabricated from re-used nickel alloy. However, the ultimate tensile strength (UTS) and yield strength (YS) remained comparable for specimens from unused and re-used powder batches.

Tang et al. [12] also observed oxygen pickup with re-using Ti-6Al-4V powder in EB-PBF which was explained to be the reason for increases in UTS and YS. The PSD became narrower with the powder re-use due to the reduction in finer particles. Fewer satellites (i.e., fine particles adhered to larger particles during atomization [1]), and consequently, fewer agglomerates were found in the re-used batch. Powder flowability was observed to increase with continuously re-using the powder due to satellites removal and longer exposure of the powder to elevated temperatures, which can decrease moisture content, and consequently, increase the flowability.

While Popov et al. [17] reported a lower fatigue performance for specimens manufactured via EB-PBF 69-times re-used Ti-6Al-4V powder as compared to the ones from unused powder, Carrion et al. [9] observed some improvements in the high cycle fatigue (HCF) behavior of LB-PBF Ti-6Al-4V specimens by heavily re-using the powder. The higher fatigue performance of specimens from re-used powder was due to the fact that cracks initiated from smaller gas-entrapped pores. The existence of less and smaller defects within the specimens fabricated from re-used powder was explained by the combination of better powder flowability and less compressibility of the re-used batch. The improved flowability resulted in a more uniform powder layer on the build plate with fewer and smaller empty spaces within the powder bulk, resulting in lower compressibility, and consequently, smaller defects within the fabricated parts.

In addition, no significant changes in the microstructure and tensile behavior of LB-PBF Ti-6Al-4V parts were observed due to powder re-use [9]. Similar fatigue lives were also obtained for the parts fabricated from unused and re-used powder batches in the as-built surface condition which was explained by the crack initiation from rough surfaces inherent to AM [19,20]. The effect of re-using 17−4 PH stainless steel (SS) powder in an LB-PBF process and nitrogen atmosphere for 15 and 11 times was investigated in two separate studies [14]. While no significant changes in the tensile behavior of parts were observed, it was reported in both studies that the apparent density and flowability of the powder could increase with re-using the powder.

Previous studies reported flowability as an important powder characteristic which can significantly affect the parts mechanical properties [9]. Flowability, however, is a complicated characteristic since it is dependent on several other powder characteristics (e.g., particle size, shape, bulk or surface chemistry, etc.) [21]. Therefore, several powder characteristics are often analyzed to illustrate flowability [8,22]. Additionally, powder characteristics can vary across the build plate due to the mechanism of powder distribution in PBF machines (i.e., spreading a powder layer upon the build plate using a recoater/wiper). Such variations in powder characteristics contribute to the complexity of understanding how the powder specification and re-use affect the mechanical performance of parts fabricated by PBF methods. Such powder characteristics can also affect the spreadability of the powder on the build plate; therefore, mechanical properties of parts fabricated in different locations of the build plate may be different [23].

It has been established that re-using powder can significantly alter the powder characteristics. Such variations may, in turn, affect the mechanical properties and challenging the qualification and certification of AM parts, specifically in safety critical applications [24,25]. Therefore, this study investigates the effects of powder re-use on the defect distribution and mechanical properties including tensile and fatigue behavior of parts fabricated from 17−4 PH SS via LB-PBF. In addition, the location of AM parts on the same build plate may contribute to variations in the final microstructural characteristics as well as mechanical performance of parts fabricated via LB-PBF. Hence, the location dependency of LB-PBF parts and how re-using the powder may affect this location dependency will also be evaluated in this study.

Table 1
Chemical composition of the argon-atomized 17-4 PH SS provided by LPW Technology Ltd.

Elements	C	Cr	Ni	Cu	Mn	Si	Nb	Mo	N	O	P	S	Fe
Wt. %	0.01	16.30	4.18	4.10	0.22	0.40	0.25	0.02	0.04	0.05	0.012	0.004	Bal.

2. Experimental program

In this study, argon-atomized 17 − 4 PH SS powder produced from LPW Technology Ltd. was used. The initial particle size distribution (PSD) was reported by the manufacturer to be between 15 and 45 μm. The chemical composition of the powder provided by the manufacturer is reported in Table 1. The study was started with an initial amount of 80 kg to guarantee 15 consecutive builds. After each fabrication, all the powder was collected from the overflow bin and build envelope and filtered through an 80-μm sieve to ensure the removal of spatters and breaking down of agglomerates. After sieving, all the powder was thoroughly mixed with the unused powder in the feed bin and a sample was taken at equal increments throughout the depth of the powder according to ASTM B215 [26] standard for powder characterizations.

Two different layouts, defined as full and half, were designed (see Figs. 1 (a) and (b)). The full layout was used for batches 1, 5, 10 and 15, while the half layout was used for the interval builds (i.e., batches 2, 3, 4, 6, 7, 8, 9, 11, 12, 13, and 14). The full layout contained 38 specimens including net-shape round specimens with a uniform gage section according to ASTM E606 [27] (see Fig. 2(a)), 11-mm square bars to be further machined to the final shape and geometry of round specimens with uniform gage section based on ASTM E606, and round tension test specimens for tensile testing according to ASTM E8 [28] (see Fig. 2(b)). The maximum testing strain was selected to be 0.0040 mm/mm; therefore, the risk of buckling under compression portion of fully reversed loading was very small. This allowed the diameter of round specimens with uniform gage section to be reduced from the standard recommended 6.25 mm to 5 mm to save in material and ensure completion of 15 builds.

Side supports were fabricated in conjunction with the net-shape specimens (see Figs. 1(a) and (b)) to prevent deflection during contact with the recoater, and thus, disturbance of the powder near the specimens. The number of specimens on the half layouts was lowered from 38 to 18 specimens. Approximately 2.5 kg and 1.5 kg powder amounts were used for the fabrication of each full and half print layouts, respectively. Most specimens were located on two ends of the build plate. Front specimens were closer to the feed bin and back specimens were further away from the feed bin (see Fig. 1(c)). This front and back specimen layout was designed in order to study the effects of part location upon the build plate on the final mechanical properties. Although there were two specimens located in the middle section of the build plate in both layouts, they were not used in this study.

All builds were fabricated using an EOS M290 machine in a nitrogen atmosphere with the manufacturer recommended 17 − 4 PH SS performance process parameters, reported in Table 2. All the specimens were subjected to CA-H1025 heat treatment. This heat treatment consists of solution treatment at 1050 °C for 30 mins, air cooling to room temperature, with a subsequent aging at 552 °C for 4 hrs and air cooling to room temperature. This heat treatment was selected since it was shown to be effective in homogenizing the microstructure and improving the fatigue performance of LB-PBF 17 − 4 PH SS specimens [29]. Net-shape round specimens were tested after heat treatment without any further surface treatments; therefore, they are referred to as as-built specimens in this study. However, the square bars were

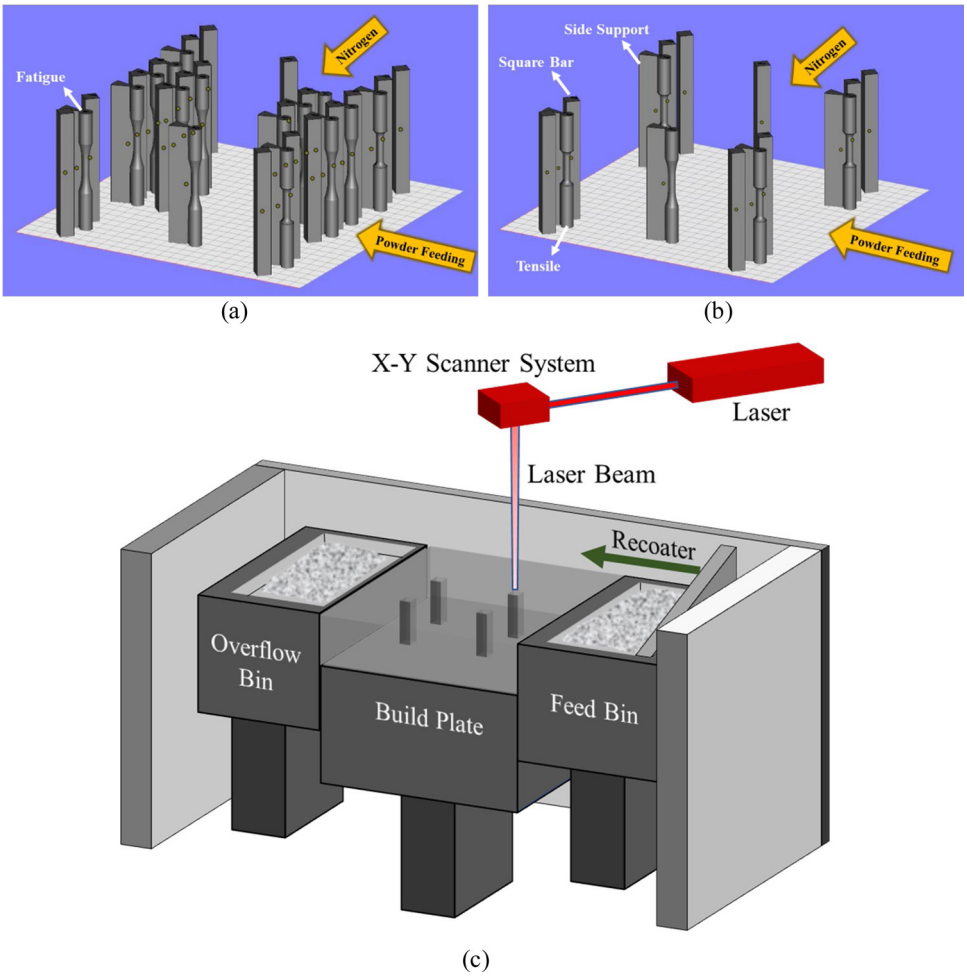

Fig. 1. (a) Full print layout used for Batch 1 (unused), Batch 5 (re-used 4 times), Batch 10 (re-used 9 times) and Batch 15 (re-used 14 times), (b) half print layout used for interval prints, and (c) a schematic of laser beam powder bed fusion (LB-PBF) system.

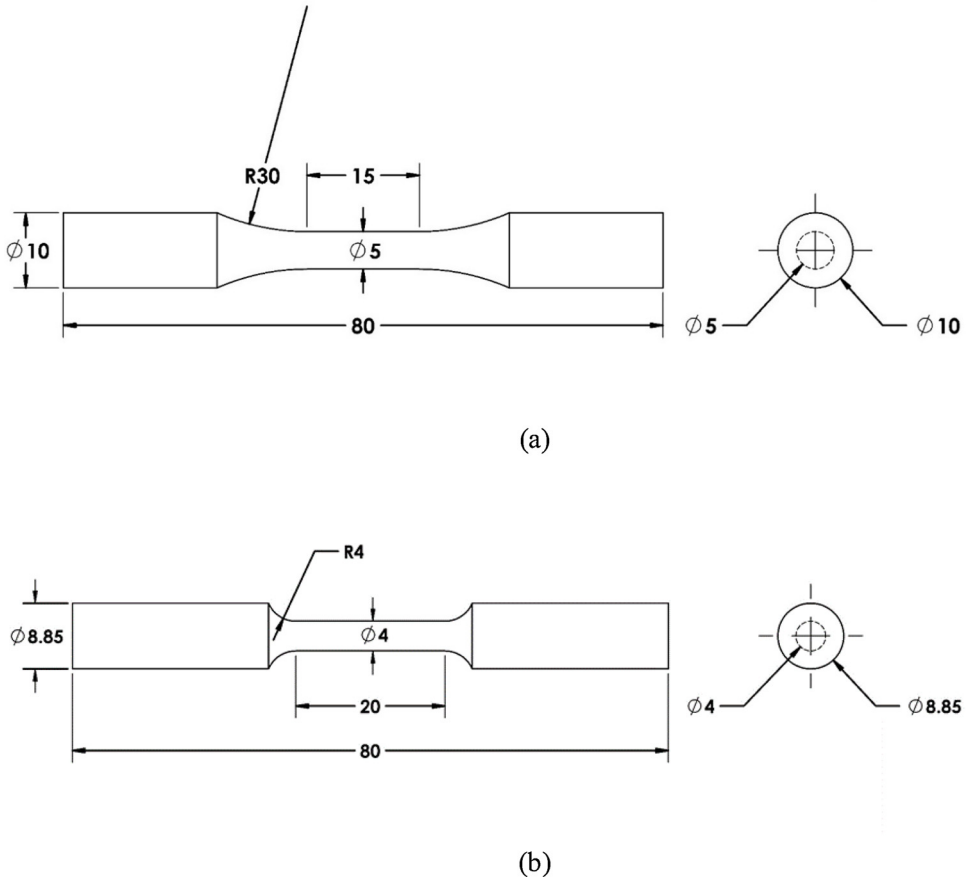

Fig. 2. (a) Round specimens with a uniform gage section for strain-controlled fatigue testing according to ASTM E606 [27], and (b) round tension test specimens for tensile testing according to ASTM E8 [28] (all dimensions are in mm).

Table 2
EOS recommended major process parameters utilized to fabricate LB-PBF 17-4 PH SS parts.

Laser power	Scanning speed	Hatch distance	Layer thickness	Layer rotation angle	Stripe width
220 W	755.5 mm/s	100 μm	40 μm	67°	100 mm

machined to the final specimen dimensions, as shown in Fig. 2(a), followed by further surface polishing to achieve $R_a = 0.5-0.6$ μm, and are referred to as machined specimens.

Powder characteristics including apparent and tapped density (i.e., the density when the powder is compacted), compressibility, shear stress [30], and cohesion were evaluated using Freeman Technology FT4 rheometer. PSD and shape morphology were analyzed via Malvern Morphology G3SE by static image analysis according to ASTM E2651 [31]. Particle shape parameters including circular equivalent (CE) diameter (i.e., the diameter of a circle with the same area as the particle's projected area on the normal plane [32]), circularity (defined as circle equivalent perimeter divided by the actual perimeter), and elongation (i.e., 1-width/length) were also measured. The powder shape morphology was also obtained with scanning electron microscopy (SEM) in order to compare unused and re-used powder batches. In this paper, the powder samples used for the full layouts are categorized into Batch 1 (i.e., unused), Batch 5 (re-used 4 times), Batch 10 (re-used 9 times), and Batch 15 (re-used 14 times).

Quasi-static tensile tests were performed via an MTS servo-hydraulic load frame with a 100 kN capacity according to ASTM E8 [28] on three specimens at a strain rate of 0.001 s^{-1}. Strain-controlled tensile tests were performed up to 0.045 mm/mm, followed by extensometer removal, and continued in displacement control until specimen failure. Fully reversed strain-controlled fatigue tests ($R_\varepsilon = -1$) according to ASTM E606 [27] were conducted on as-built specimens at two different strain amplitudes, ε_a, of 0.0040 mm/mm and 0.0020 mm/mm to study low and high cycle fatigue regimes, respectively. Strain amplitudes of 0.0025 mm/mm, 0.0030 mm/mm, and 0.0040 mm/mm in fully reversed condition ($R_\varepsilon = -1$) were used for machined specimens to evaluate their high, intermediate (or mid), and low cycle fatigue regime behaviors, respectively. In this study, low cycle fatigue (LCF) and high cycle fatigue (HCF) regimes are associated with high and low strain amplitudes. At least, two specimens were tested at each strain level to check the repeatability of the results. The frequency at each strain level was adjusted to maintain similar average cyclic strain rates among all tests to minimize any variations due to strain dependent deformation effects.

Fracture surfaces were analyzed via a Keyence VHX-6000 digital microscope to investigate the shape and size of the crack initiation sites. In addition, porosity measurements were carried out by serial cross-section analysis of specimens from Batch 1 and Batch 15 and analyzed using the Keyence VHX-6000 digital microscope at 500X to compare the porosity of the produced parts. Surface roughness of the specimens was also measured using Mahr MFW-250, which consists of a stylus instrument traversing perpendicular to the surface at constant speed to measure the surface profile for calculating the roughness parameters.

3. Experimental results

3.1. Powder characteristics

One of the most important characteristics of the powder particles is their size and shape morphology which may affect physical properties of the powder such as flowability. The PSD diagrams of Batches 1, 5, 10 and 15 are shown in Fig. 3. An enhanced view of PSD for finer particles (smaller than 15 μm) is also included. Although the variation in PSD between powder batches does not appear to be significant, powder re-use results in the PSD diagram to become somewhat narrower (the width of PSD was 45 μm for Batch 1 and 41 μm for Batch 15) and the circular equivalent (CE) diameter slightly decreases with continued powder re-use (it was measured as 30.8 μm for Batch 1 and 28.4 μm for Batch 15).

The difference in CE diameters can be related to the sieving and manufacturing processes. The large agglomerates can get detached or break down by the filtration. The reduction of large agglomerates was verified by D_{90} measurement which gives the particle size below which 90 % of the sample lies [1]. The D_{90} was measured to decrease from 43.40 μm in Batch 1 to 40.20 μm in Batch 15. Very fine particles can also spatter (be ejected) from the build plate when the laser scans that area and/or they may be included in the melting and subsequent solidifying process [9]. The number of very fine particles (smaller than 15 μm) was found to decrease with re-using the powder from 9 % to 6 % of the powder samples. Therefore, as the satellites are shed from the agglomerates, the CE diameter will become more representative of the parent particle rather than the cluster of particles. Powder flowability and packing state may improve by the reduction of very fine particles and large agglomerate due to relatively high interparticle frictional forces of fine particles and empty spaces between agglomerates [1,9,12].

The shape morphology of powder particles captured via SEM is shown in Fig. 4. No apparent change in shape can be observed as a result of continuous powder re-use. It can also be observed that most particles remained spherical after re-using the powder. This was verified by measuring the particles' circularity which was comparable for all the powder batches (0.87 − 0.88). Elongated particles can cause friction between particles which may impede the flow [1]. Therefore, having less elongated particles in the powder batch can contribute toward a better powder flowability. Needles have elongation (1-width/length) values approaching to 1. The particles' elongation was measured to be 0.20 for Batch 1 and 0.19 for Batch 15. Hence, no effect of re-using the powder on elongation was found in this study.

Apparent/bulk and tapped density values of the powder batches have been listed in Table 3. The bulk density shows an increase with continuous powder re-use. Tapped density was also increased slightly with re-using the powder. The increase in bulk and tapped densities can be due to existence of fewer agglomerates in the re-used powder batch resulting in less empty spaces within the powder batch. It should be noted that although finer particles can fill in the void/empty spaces between the larger particles [1], they may also adhere to large particles due to their larger interparticle frictional forces and cohesivity [9], form more agglomerates, and leave empty spaces in the powder bulk. As a result, the larger apparent and tapped density values of the re-used powder batches can be due to a more uniform particle size distribution and better packing state.

The existence of more empty spaces within the powder bulk can lead to more gas entrapment during melting/solidification, which can form gas-entrapped pores in the material during melting/solidification process. The compressibility of a powder bulk can increase due to more empty spaces between the powder particles. Hence, the compressibility of all batches was measured, and it was observed that the compressibility of Batch 1 was 4.65 % compared with 1.97 % for Batch 15. This means that Batch 1 is more compressible. The higher sensitivity of Batch 1 to compression can indicate the existence of more empty spaces within the Batch 1 powder bulk. As a result, it may be postulated that the existence of more agglomerates and very fine particles, and subsequently, higher cohesion within Batch 1 can result in more empty spaces entrapped within the powder bulk [1,9].

To verify this understanding, permeability of different powder batches was quantified. Permeability indicates how easily a gas (i.e., nitrogen) can flow through a material (i.e., powder) [32]. Permeability is inversely correlated with pressure drop due to applied normal stresses on the powder bulk [9,32]. This means that powder with a greater pressure drop is the least permeable one. As seen in Fig. 5, pressure drop in Batch 15 is higher than all the other batches. This may imply that the Batch 15 is the least permeable powder. As it was explained by the differences in compressibility values between different powder batches, nitrogen gas can flow more easily within Batch 1 and least easily within Batch 15. The higher permeability of nitrogen within Batch 1 is mainly due to more empty spaces and less barriers due to agglomerations existence within the powder batch, which leads to a relatively smaller pressure drop (see Fig. 5), less apparent and tapped densities (see Table 3), and more compressibility. However, in Batch 15, with less agglomerates, there are fewer empty spaces, and therefore, gas has more difficulties going through the powder batch, which in turn increases the pressure drop.

A method to show the higher cohesion and interparticle frictional forces within Batch 1 compared with other batches is to perform shear cell test. In shear cell test, powder is sheared to obtain its shear strength properties [33]. Higher shear strength represents higher resistance for powder to flow [32], and thus, less flowability resulting in less uniform powder distribution on the build plate. Shear cell tests were performed according to ASTM D7891 [30] at applied normal stresses up to 2 kPa. It can be observed from Fig. 6 that Batch 1 has the highest shear stress under different normal stress levels. Additionally, the cohesion within each powder batch was measured to be 0.250 kPa for Batch 1 compared with 0.128, 0.158, and 0.160 kPa respectively for Batches 5, 10, and 15. This shows that at a constant applied normal stress (e.g., powder stored in the feed bin can experience a consolidation stress), Batch 1 requires more shear stress in order to flow due to higher cohesivity.

3.2. Porosity within the fabricated parts

Pores at the gage section of representative specimens fabricated from Batch 1 (i.e., unused) and Batch 15 (i.e., re-used 14 times), one from the front and one from the back of the build plate, were measured via digital microscopy and their size distributions are presented in Fig. 7. Porosity measurements were conducted on three different cross sections at the gage of each representative specimen. Pores with diameters smaller than 5 μm were disregarded from this analysis since they

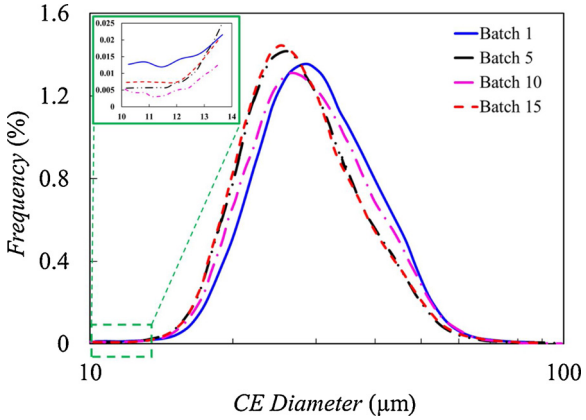

Fig. 3. Particle size distribution (PSD) of Batch 1 (unused), Batch 5 (re-used 4 times), Batch 10 (re-used 9 times), and Batch 15 (re-used 14 times) showing the PSD becomes slightly narrower and shifts to the left by re-using the powder.

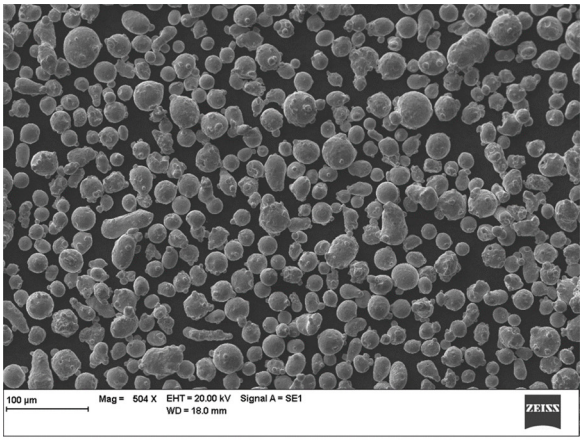

(a)

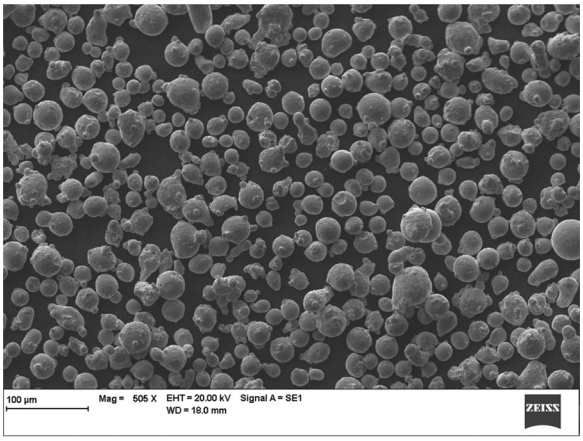

(b)

Fig. 4. Powder shape morphology for (a) Batch 1 and (b) Batch 15 obtained via SEM.

Table 3
Apparent/bulk and tapped density values of Batches 1, 5, 10, and 15.

Powder batch	Batch 1	Batch 5	Batch 10	Batch 15
Bulk density (g/mL)	3.87	4.03	4.14	4.19
Tapped density (g/mL)	4.37	4.38	4.40	4.44

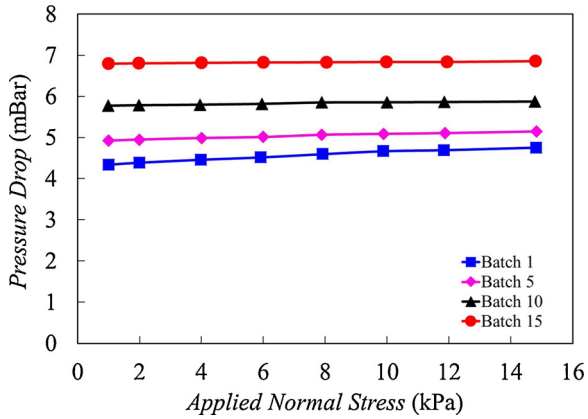

Fig. 5. Pressure drop versus applied normal stress on the powder bulk for Batches 1, 5, 10, and 15 showing the highest pressure drop for Batch 15 and the lowest for Batch 1.

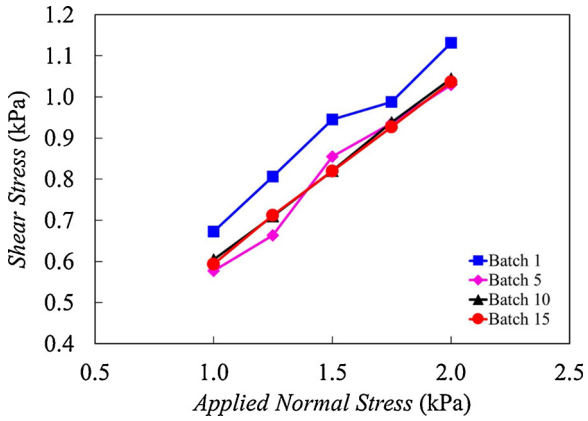

Fig. 6. Shear stress versus applied normal stress on the powder bulk for Batches 1, 5, 10, and 15 showing a higher shear stress for Batch 1 as compared to the other batches.

have relatively small probabilities to initiate a fatigue crack considering the maximum pore sizes observed. The average and maximum pore diameters for the specimen from Batch 1 in front (see Fig. 7(b)) were found to be 9.4 and 26.6 µm, respectively. Similar analysis on the gage section of a specimen from Batch 1 in back (see Fig. 7(a)) resulted in average and maximum pore dimeters of 10.4 and 33.7 µm.

The number of pores was also obtained and found to be relatively higher for the specimen in back compared with the front one (~14 % increase). Comparable procedures were also performed on specimens from Batch 15 in back and front (see Figs. 7(c) and (d)). It was found that the number of pores was relatively lower for the specimen in back by 5%. However, the average and maximum pore diameters were still larger in the specimen from Batch 15 in back compared with the specimen in front. The average and maximum pore diameters were 9.2 and 24 µm for the specimen in front and 9.8 and 29.8 µm for the specimen in back. It should be noted that the number of pores reported is the average of the number of pores found on each section. It is also worth noting that the maximum pore size reported in Fig. 7 is the maximum found on the 3 sections cut from each specimen and does not necessarily represent the maximum pore size in the specimen.

It can be concluded that the pore sizes are relatively larger for the specimens fabricated from Batch 1 compared with the counterparts from Batch 15. The decrease in pore sizes of specimens fabricated from re-used powder can be related to the lower compressibility, and consequently, the better packing state of re-used powder compared with the unused powder which results in denser parts. In addition, the number and size of pores for the unused powder specimen in back were relatively larger than the specimen in front. However, the differences between the number and size of pores in front and back specimens were decreased with continuously re-using the powder which indicates more layer uniformity of re-used powder. Hence, it can be assumed that powder flowability improved by continuous powder re-use, which resulted in the reduction of finer particles and agglomerates, as discussed in the previous section.

3.3. Tensile behavior

Tensile behavior of LB-PBF 17−4 PH SS specimens fabricated from Batches 1, 5, 10, and 15 from different locations (one from back and two from front for each batch) in as-built condition is shown via engineering stress versus engineering strain and engineering stress versus displacement curves in Figs. 8(a) and (b), respectively. One curve for each batch is presented in these figures due to negligible changes on tensile behavior as a result of specimen's location on the build plate. As seen in Fig. 8, no significant effect on tensile properties including UTS and YS was observed due to powder re-use either. The UTS was found to

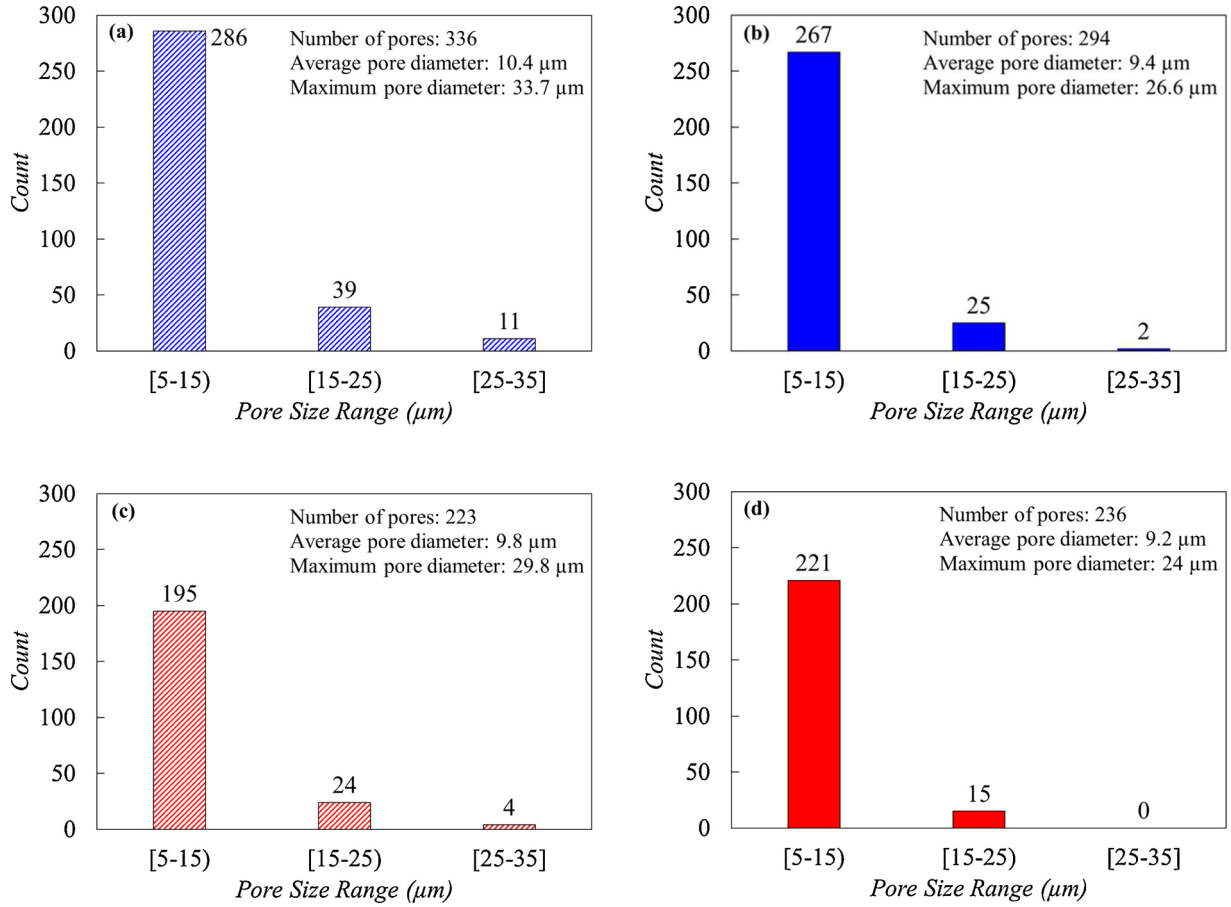

Fig. 7. Pore size distribution obtained from multiple cross sections at the gage of the specimens from (a) Batch 1 in back, (b) Batch 1 in front, (c) Batch 15 in back, and (d) Batch 15 in front.

remain comparable around 1203 MPa for Batch 1 and 1193 MPa for Batch 15. The YS was also measured according to 0.2 % offset approach, and it was found to be 1155 and 1138 MPa for Batch 1 and 15, respectively. It should be noted that the tensile properties were obtained from the previous work of authors.

True fracture strain, ε_f, was also measured by $ln(\frac{A_0}{A_f})$, in which A_0 and A_f are initial and fracture cross-sectional areas of the gage [34]. The true fracture strain was found to be 0.35 and 0.40 for specimens fabricated from Batch 1 and 15, respectively, showing relatively higher ductility with continuously re-using the powder which can be related to the lower porosity in specimens from re-used powder. Since no difference in microstructure of the specimens fabricated from unused and re-used powder was expected due to powder re-use and heat treatment [9,29], changes in material strength were expected to be negligible. A summary of the main tensile properties is provided in Table 4.

3.4. Fatigue behavior

Strain-controlled fully reversed ($R_\varepsilon = -1$) tests were performed on both as-built and machined specimens fabricated from unused and re-used powder batches. The effect of specimen location on the build plate on the fatigue behavior was also investigated by comparing samples from the same batch, however, with different locations; i.e., front or back. A summary of strain-controlled fatigue test results for specimens fabricated from 17−4 PH SS via LB-PBF in as-built and machined conditions and heat treated utilizing CA-H1025 procedure is presented in Tables 5 and Table 6, . respectively. Results are categorized for different batches and from two different locations (i.e., front versus back). Cyclic modulus of elasticity of the stable cycle, E', strain amplitude, ε_a, mid-life stress amplitude, σ_a, and mean stress, σ_m, as well as number of reversals to failure, $2N_f$, are included in Tables 5 and Table 6. It is important to mention that no substantial plastic deformation occurred for any of the LB-PBF 17−4 PH SS specimens in this study

Strain-life comparison of specimens in the as-built condition form different batches is shown in Fig. 9. Fatigue lives are presented on a semi-log plot with strain amplitude, ε_a, on Y axis and number of reversals to failure, $2N_f$, on X axis. Specimens were tested in two different strain levels. As seen in Fig. 9, no effect of powder re-use was observed on the fatigue life of specimens with as-built surface condition. In addition, no effects of location (i.e., front versus back location) on fatigue life of LB-PBF specimens in the as-built surface condition can be observed from this figure. Therefore, no specific trend in fatigue life as a result of re-using the powder nor location was observed when specimens were kept in their as-built surface condition.

Strain-life fatigue behavior comparison of LB-PBF CA-H1025 17−4 PH SS specimens from Batch 1 and Batch 15 fabricated in front location (i.e., closer to the feed bin) and in machined surface condition is shown in Fig. 10(a). Due to the stochastic nature of the defect size and number in the specimens, the fatigue lives show greater scatter in the machined surface condition as compared to the as-built surface condition. It can be seen that continuously re-using the powder did not affect the fatigue behavior in low cycle fatigue (LCF) and mid cycle fatigue (MCF) regimes. In the high cycle fatigue (HCF) regime, however, a gap between fatigue lives of machined specimens fabricated from Batch 1 and Batch 15 can be observed. In this regime, fatigue life appears to be improved by re-using the powder. A similar trend was also observed in Fig. 10(b) for the machined specimens fabricated from Batch 1 and 15 in the back location (i.e., further away from the feed bin). As shown in Fig. 10(b), the variation between the results is not significant in LCF and MCF

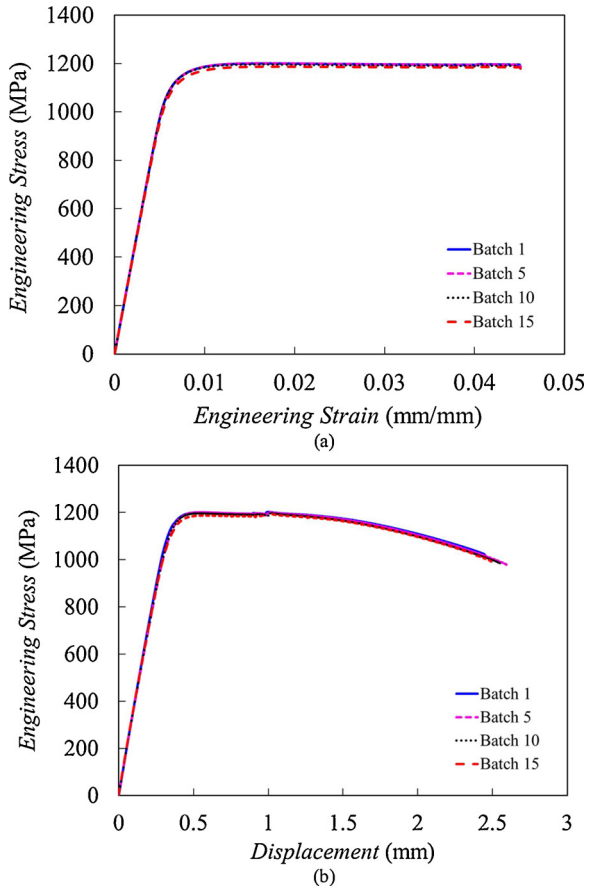

Fig. 8. Tensile behavior of LB-PBF CA-H1025 17-4 PH SS specimens fabricated from Batches 1, 5, 10, and 15 in the as-built surface condition: (a) engineering stress-strain and (b) engineering stress-displacement curves adapted from.

Table 4
LB-PBF CA-H1025 17-4 PH SS tensile properties obtained from as-built specimens.

Batch	*UTS* (MPa)	*YS* (MPa)	ε_f (mm/mm)
1	1203	1155	0.35
5	1201	1151	0.42
10	1198	1156	0.44
15	1193	1138	0.40

regimes, although it can be seen that specimens fabricated from Batch 15 had slightly longer fatigue lives compared with the ones from Batch 1. However, the HCF lives were improved by continuously re-using the powder. In addition, the difference observed in the HCF data between specimens fabricated by unused and re-used powder batches in the back location was more significant as compared to the counterparts from front location (compare Figs. 10(a) and (b)).

The effect of part location on the build plate on the fatigue lives of LB-PBF CA-H1025 17−4 PH SS machined specimens is shown in Figs. 11(a) and (b), respectively for Batch 1 and Batch 15. The effect of powder re-use on the fatigue behavior of specimen is ruled out by considering the specimens from the same batch but different locations. As it can be observed from Figs. 11(a) and (b), the fatigue lives of specimens from front location are relatively greater than the ones from back location, independent of strain level. It can be observed from Fig. 11(b) that the gap between fatigue lives of front and back location specimens was reduced with continuous re-use of the powder. It may be presumed that specimens from front location consistently have a greater fatigue life compared with the ones from back location;

Table 5
Strain-controlled fully reversed fatigue test results obtained from LB-PBF CA-H1025 17-4 PH SS specimens in as-built surface condition.

	Location	E' (GPa)	ε_a (mm/mm)	σ_a (MPa)	σ_m (MPa)	$2N_f$ (Reversals)
Batch 1						
As-built	Back	194	0.0040	797	44	6,154
As-built	Front	198	0.0040	801	−5	9,844
As-built	Front	201	0.0020	407	−5	174,348
As-built	Back	199	0.0020	401	−3	200,654
As-built	Back	201	0.0020	405	−5	203,878
Batch 5						
As-built	Front	196	0.0040	801	−11	10,178
As-built	Back	196	0.0040	801	−8	10,480
As-built	Front	188	0.0020	382	−2	58,550
As-built	Front	201	0.0020	407	4	62,434
As-built	Back	199	0.0020	403	−4	98,038
As-built	Front	199	0.0020	401	−1	191,532
Batch 10						
As-built	Back	196	0.0040	793	−4	9,370
As-built	Front	196	0.0040	797	−4	11,150
As-built	Front	199	0.0020	401	4	75,996
As-built	Front	198	0.0020	402	−1	117,696
As-built	Back	198	0.0020	398	−2	209,518
Batch 15						
As-built	Back	196	0.0040	797	−1	12,982
As-built	Front	197	0.0040	801	−10	13,450
As-built	Front	200	0.0020	400	−3	97,847
As-built	Front	200	0.0020	403	−5	230,788
As-built	Back	199	0.0020	401	−1	235,294

Table 6
Strain-controlled fully reversed fatigue test results obtained from LB-PBF CA-H1025 17-4 PH SS specimens in machined surface condition.

	Location	E' (GPa)	ε_a (mm/mm)	σ_a (MPa)	σ_m (MPa)	$2N_f$ (Reversals)
Batch 1						
Machined	Back	200	0.0040	812	17	10,564
Machined	Back	201	0.0040	811	−9	14,146
Machined	Front	200	0.0040	814	−16	63,300
Machined	Front	199	0.0040	805	−14	69,988
Machined	Back	199	0.0030	603	−4	76,638
Machined	Back	203	0.0030	612	−3	97,828
Machined	Back	205	0.0025	512	11	100,492
Machined	Back	205	0.0025	518	−41	193,634
Machined	Front	201	0.0030	609	−1	287,624
Machined	Front	197	0.0030	603	−24	459,082
Machined	Front	203	0.0025	510	−6	1,747,292
Machined	Front	201	0.0025	508	12	9,194,508
Batch 15						
Machined	Back	196	0.0040	801	−14	24,978
Machined	Back	202	0.0040	826	−33	31,044
Machined	Front	203	0.0040	823	10	59,298
Machined	Front	204	0.0040	823	−11	66,154
Machined	Back	204	0.0030	619	−2	118,476
Machined	Front	203	0.0030	615	1	119,494
Machined	Back	199	0.0030	599	−2	150,470
Machined	Front	205	0.0030	621	15	304,992
Machined	Back	203	0.0025	514	18	4,523,250
Machined	Back	199	0.0025	505	1	6,379,896
Machined	Front	202	0.0025	508	−4	15,084,902
Machined	Front	202	0.0025	510	−16	18,417,542

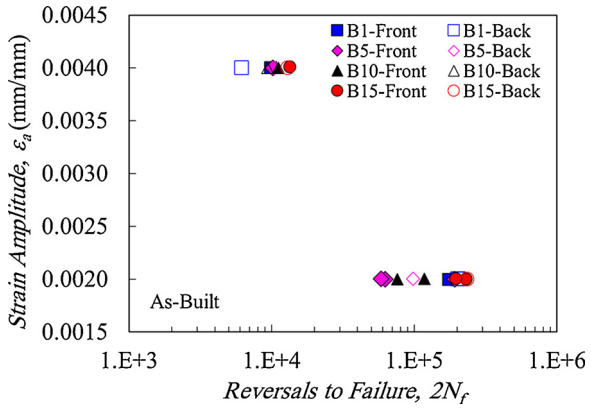

Fig. 9. Strain-life fatigue behavior of LB-PBF CA-H1025 17-4 PH SS specimens in the as-built surface condition fabricated from Batch 1 (B1), Batch 5 (B5), Batch 10 (B10), and Batch 15 (B15) in front and back locations.

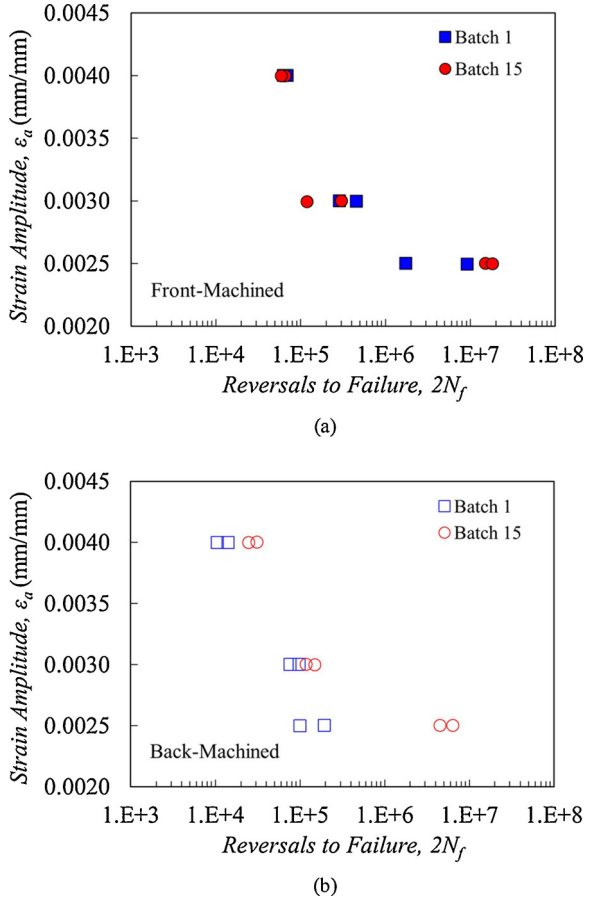

Fig. 10. Strain-life fatigue behavior of LB-PBF CA-H1025 17-4 PH SS specimens in machined surface condition fabricated from Batch 1 and Batch 15 in (a) front and (b) back locations.

however, such differences are reduced by re-using the powder.

3.5. Failure analysis

Fractography analysis via digital microscopy was performed on the fracture surfaces of as-built and machined specimens from different locations. It was observed that in all as-built specimens, cracks started from the micro notches on the surface of the specimens due to rough surfaces inherent to the LB-PBF process. This was consistent for specimens from different batches regardless of the powder re-using iteration

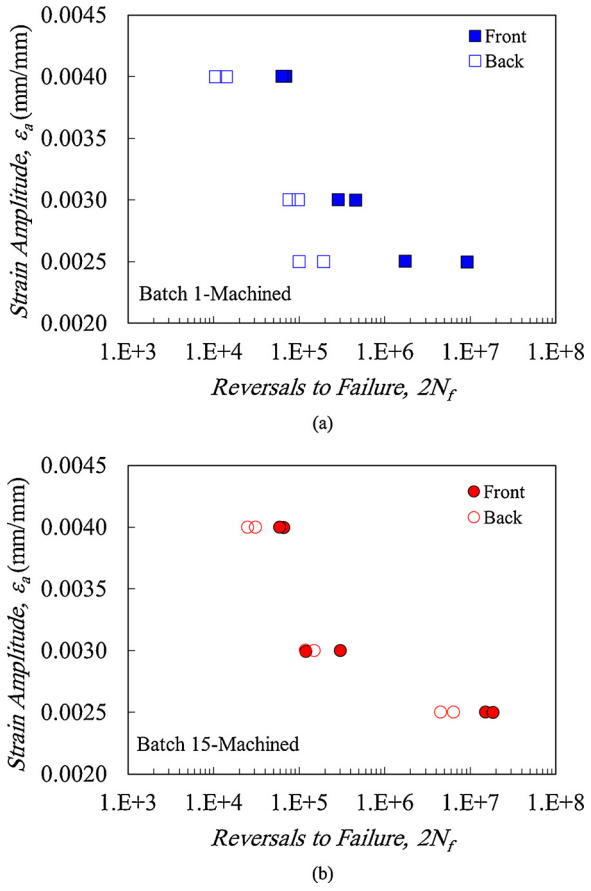

Fig. 11. Strain-life fatigue behavior of LB-PBF CA-H1025 17-4 PH SS specimens in machined surface condition fabricated from (a) Batch 1 and (b) Batch 15 in front and back locations.

or specimen location. Fracture surface of an as-built specimen fabricated from Batch 1 in front and tested at ε_a= 0.0040 mm/mm with 9,844 reversals to failure is shown in Fig. 12(a). A focused view of the fracture surface is also presented in the excised area. As shown in this figure, cracks have initiated from multiple locations and even different layers (shown by white arrows), propagated, coalesced to form a larger crack and continued to propagate until the part failed.

The fracture surface of a Batch 1 counterpart from the back location at ε_a= 0.0040 mm/mm with 6,154 reversals to failure is shown in Fig. 12(b). A similar trend was observed that cracks initiated from multiple locations at different layers and coalesced before final part failure. In Fig. 12(c), a specimen fabricated from Batch 15 and front location at ε_a= 0.0040 mm/mm is shown with 13,450 reversals to failure. Although this specimen had a longer fatigue life compared with its counterpart from Batch 1 at the same strain level, a similar trend in fatigue failure was observed in which cracks initiated from multiple locations and different layers. Similar failure mechanism was also observed for the specimens tested at ε_a= 0.0020 mm/mm. All cracks initiated from multiple locations on the surface, although there was more scatter in data at this strain level.

A comparable procedure was performed for specimens in the machined surface condition from different locations and powder batches to analyze their fracture surfaces. It was observed that cracks usually started from internal pores or the pores that were brought closer to the surface due to machining. As seen in Fig. 13(a), cracks initiated from two gas-entrapped pores close to the surface of a specimen fabricated from Batch 1 in front with 1,747,292 reversals to failure at ε_a= 0.0025 mm/mm. The crack initiation site is illustrated with white arrow. A close-up of the crack initiation site is also shown in the same figure

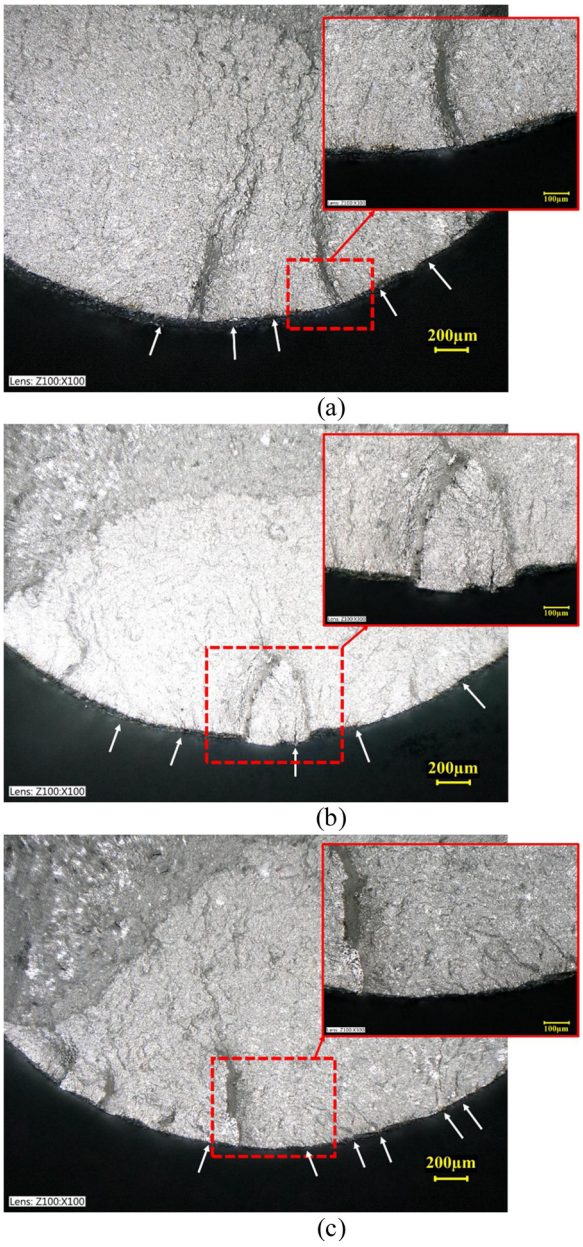

Fig. 12. Fracture surfaces of LB-PBF CA-H1025 17-4 PH SS specimens in as-built surface condition from (a) Batch 1 and front with 9,844 reversals to failure, (b) Batch 1 and back with 6,154 reversals to failure, and (c) Batch 15 and front with 13,450 reversals to failure, all tested at 0.0040 mm/mm strain amplitude.

detailing the characteristics of the defects associated with crack initiation. In the close-up, it can be observed that the crack initiated from the two gas-entrapped pores with spherical shape and in proximity of each other which were brought close to the surface by machining.

Figure 13(b) shows a specimen from the same powder batch however from the back location and 100,492 reversals to failure at the same strain amplitude of ε_a= 0.0025 mm/mm. Cracks were observed to be initiated from a lack-of-fusion (LoF) defect shown by white arrow which was brought to the surface by machining. Additionally, multiple LoF defects were observed on the fracture surface of this specimen which are shown by yellow arrows. Interestingly, no LoF defect was found during the porosity analysis for which the results are presented in Fig. 7. This can be explained by the fact that LoF defects are slit shaped and do not have much heights and they occur between two consecutive layers, which is 40 μm (as the powder layer thickness) for the LB-PBF 17−4 PH SS specimens fabricated in this study. The porosity size distributions in this study were performed by randomly cutting the gage section of representative specimens throughout the gage length and in radial direction and observing the cut section under microscope to count and measure pores. Considering the shape and spacing of these potential LoF defects, it is very easy to miss them during the porosity analysis performed in this study.

Fracture surfaces of machined specimens from Batch 15 fabricated in front and back locations were also analyzed using the same approach. Fracture surface of LB-PBF specimen fabricated from Batch 15 in front at ε_a= 0.0025 mm/mm with 15,084,902 reversals to failure is presented in Fig. 14(a). An enhanced view of the crack initiation site is also included. It can be observed that cracks initiated from a spherical pore close to the surface, shown by white arrow, of the front location specimen resulting in the part failure. Similar analysis on the fracture surface of a machined specimen from Batch 15 and fabricated in the back location at ε_a= 0.0025 mm/mm with 4,523,250 reversals to failure at the same strain amplitude is shown in Fig. 14(b). This image indicates that the cracks initiated from an internal LoF defect, which led to the part failure. The LoF defect is also shown by white arrow.

It was observed that failure was occurred comparably in the specimens fabricated from Batch 1 and 15 and from the front location (see Fig. 13(a) and Fig. 14(a)). In these specimens, failure was due to crack initiations from gas-entrapped pores. However, in the specimens fabricated from Batch 1, cracks consistently initiated from larger gas-entrapped pores under the same strain amplitudes. In addition, the cracks were observed to initiate from gas-entrapped pores (usually spherical) in the specimens located in the front location regardless of the powder batch used. However, failure occurred by larger irregular shaped LoF defects in the specimens from the back. Therefore, it may be assumed that even on the same build plate, parts can have distinctly different performances due to the variation of powder characteristics in different locations.

The cracks initiated similarly from LoF defects in the specimens fabricated in the back of the build plate from both Batch 1 and Batch 15. However, as shown in Fig. 13(b), the LoF defect was larger compared with the defect in the specimen fabricated from Batch 15 and same location (see Fig. 14(b)). This trend was observed for all the specimens analyzed in this study. The specimen fabricated from Batch 1 and from the back had a much shorter fatigue life as compared to the specimen from Batch 15 and the comparable location at the same strain amplitude. Therefore, in all the specimens with similar location and strain amplitude, cracks initiated from relatively larger defects (i.e., gas-entrapped pore or LoF) in the specimens fabricated from unused powder compared with the specimens from re-used powder. The larger defects in specimens fabricated from unused powder resulted in shorter fatigue lives compared with the counterparts fabricated from re-used powder. Moreover, in the specimens from the same batch, the defects were gas-entrapped pores in the specimens in front while there were more LoF defects in the specimens located in back.

4. Discussion on experimental results

Tensile monotonic behaviors of specimens from different batches were presented in Fig. 8 and Table 4. No significant variation in tensile properties including UTS and YS due to powder re-use nor location was observed. Similar observations have been made for specimens fabricated from unused and re-used powder via LB-PBF Ti-6Al-4V [9], Inconel 718 [13], and 17−4 PH SS [14] showing comparable tensile strength with re-using the powder. Comparable tensile behaviors obtained in this study may be resulting from the limited effects powder re-using has on the microstructure and chemical composition of the fabricated parts [9,17]. However, the true fracture strain was observed to slightly increase with continuously re-using the powder, which may be explained by relatively less porosity in specimens fabricated from re-used powder as compared to the ones fabricated from unused powder,

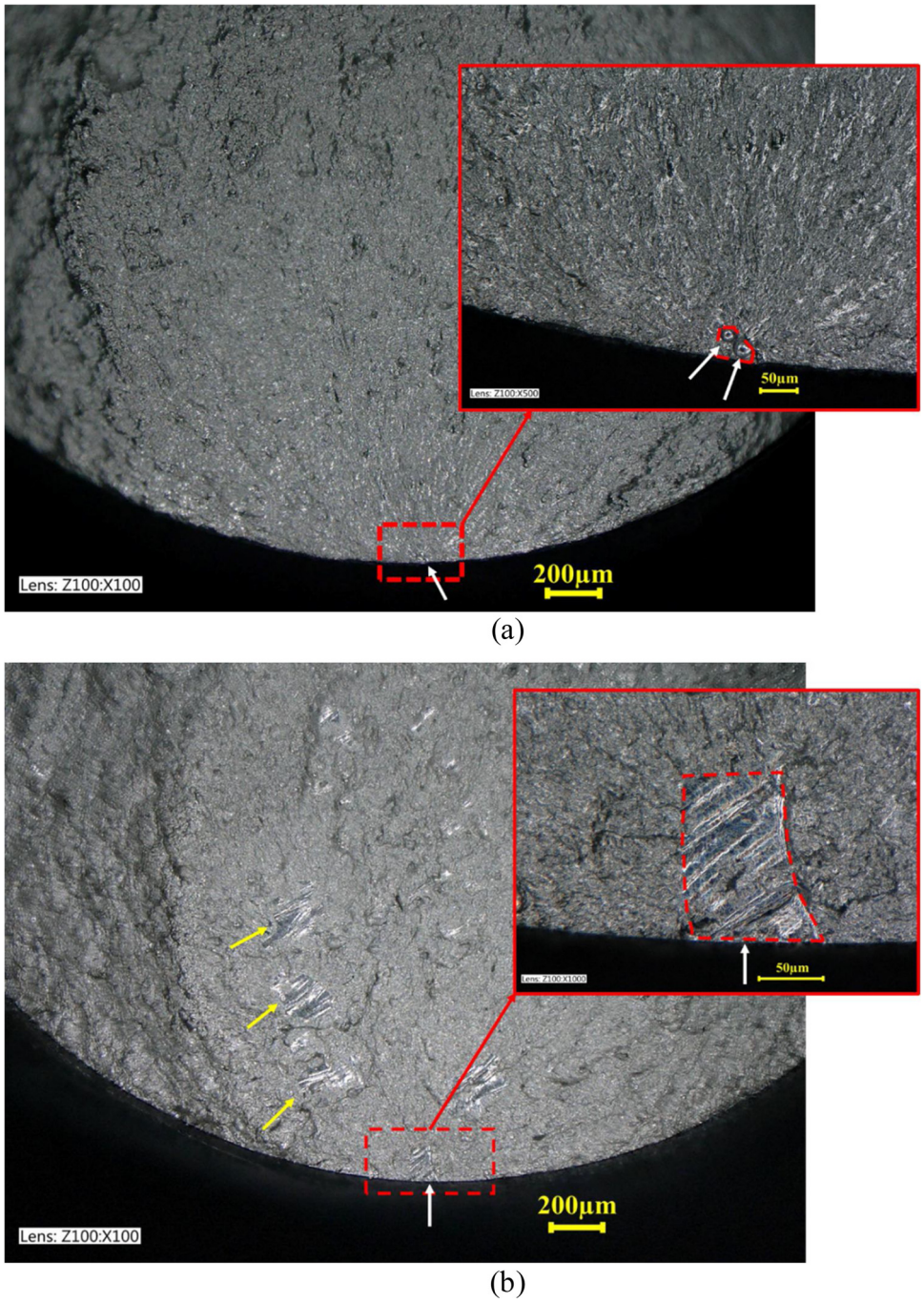

Fig. 13. Fracture surfaces of LB-PBF CA-H1025 17-4 PH SS specimens in machined surface condition fabricated from (a) Batch 1 and front with 1,747,292 reversals to failure, and (b) Batch 1 and back with 100,492 reversals to failure, both tested at 0.0025 mm/mm strain amplitude.

as evident from Fig. 7.

Fatigue testing of CA-H1025 17 − 4 PH SS parts fabricated via LB-PBF in the as-built surface condition showed no significant trend in fatigue life as a result of powder re-use (see Fig. 9). The reason can be explained by crack initiation sites from rough surfaces of as-built specimens, which act as micro notches and dominate the fatigue behavior [19] (see Fig. 12). Although average surface roughness, R_a, is not the most representative surface parameter for the fatigue behavior [35], R_a was measured for 12 specimens from different batches and locations, and all the measurements were around 7 − 9 µm. Not only did the surface roughness dominate the effects of powder re-use, but it also surpassed the effects of front and back locations (see Fig. 9) when the specimens were kept in their as-built surface condition.

In the machined surface condition, there was an observable difference between the fatigue lives of parts fabricated from Batch 1 and Batch 15 at the same location (see Figs. 10(a) and (b)) in the HCF regime. An improved fatigue resistance was observed for the specimens fabricated from Batch 15 at $\varepsilon_a = 0.0025$ mm/mm compared with the ones from Batch 1 at the same strain level. This behavior may be explained by the importance of the crack initiation stage in the HCF regime, which dominates the fatigue degradation process [34]. Cracks typically initiate from defects especially the ones that are closer to the surface or brought to the surface by machining. Therefore, the projected area of the crack-initiating defect on the loading plane from the fractography analysis was measured and the defect size was calculated based on Murakami's approach [36]. In this approach, the defect size is

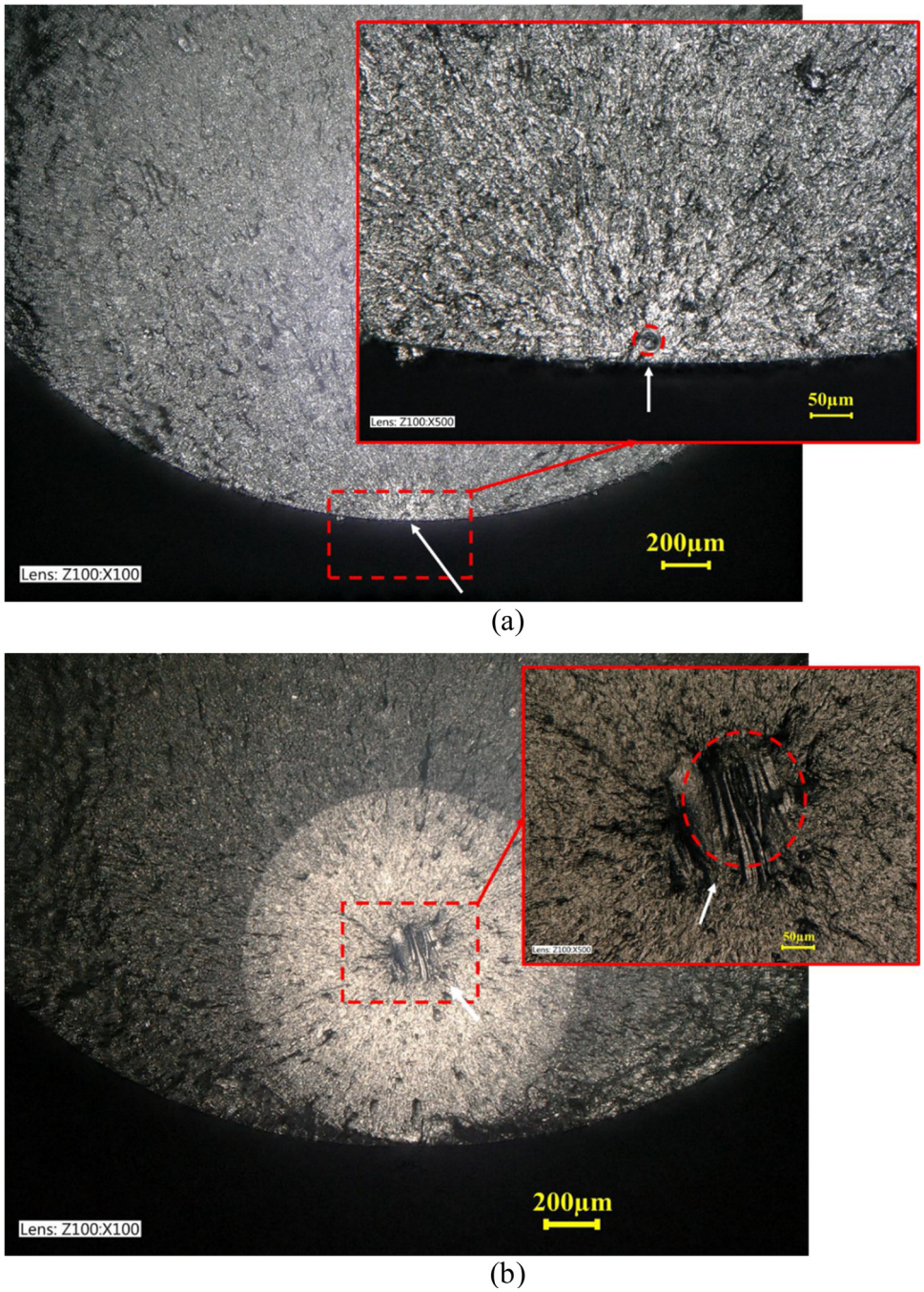

Fig. 14. Fracture surfaces of LB-PBF CA-H1025 17-4 PH SS specimens in machined surface condition fabricated from (a) Batch 15 and front with 15,084,902 reversals to failure, and (b) Batch 15 and back with 4,523,250 reversals to failure, both tested at 0.0025 mm/mm strain amplitude.

presented by the square root of the projected area on the loading plane.

The defect diameter in the normal plane was measured to be 73 µm (surface defect) for the specimen fabricated from unused powder in front with 1,747,292 reversals to failure (see Fig. 13(a)). This defect was much larger than the maximum pore size observed in Fig. 7(b) since the crack initiated from two gas-entrapped pores close to each other, and both pores were considered to estimate the effective defect diameter. It should be noted that the maximum pore size reported in Fig. 7 is the maximum found from a 2D analysis by limited sectioning and does not necessarily represent the maximum defect size in the specimen. The defect diameter was 34 µm for the specimen fabricated from re-used powder and on the front of the build plate, resulting in 15,084,902 reversals to failure (see Fig. 14(a)).

Comparably, the defect diameters were calculated for the specimens fabricated from Batch 1 and Batch 15 in the back. The defect diameter was measured to be 90 µm (surface LoF defect) for the specimen fabricated from Batch 1 in back location with 100,492 reversals to failure (see Fig. 13(b)), while it was 69 µm (internal LoF defect) for the specimen fabricated from Batch 15 in the back with 4,523,250 reversals to failure (see Fig. 14(b)). Internal defects are considered to be more than the estimated defect diameter away from the surface, while a defect is known as a surface defect when its distance to the surface is less than its diameter. In the case of surface defects, the area between the defect and surface of the part is also considered in the area calculations. Therefore, internal defects with comparable sizes to surface defects are expected to be less detrimental to fatigue failures. In addition, the average diameter of crack-initiating defects for all the specimens fabricated from unused powder in front and back at $\varepsilon_a = 0.0025$ mm/mm was 60 µm and 88 µm,

respectively. The average diameter of crack-initiating defects of all re-used powder specimens at $\varepsilon_a = 0.0025$ mm/mm was relatively smaller than unused powder specimens, and measured to be 31 μm and 64 μm respectively for front and back specimens.

Additionally, it was observed from Fig. 7 that the maximum pore diameters are consistently smaller in the specimens fabricated from Batch 15 compared with Batch 1; about 9% and 12 % smaller for the specimens in front and back, respectively. Moreover, the average pore diameters slightly decreased for the specimens fabricated from Batch 15 compared with the specimens from Batch 1 independent of location. The decrease in maximum and average pore sizes of the Batch 15 specimens can be attributed to the lower compressibility of Batch 15 as compared to Batch 1, derived from the reduction of agglomerates by powder re-use. This reduction in compressibility insinuates that the powder is naturally in a better packed state with fewer gaps between powder particles. This more uniform packing state during the melting and solidifying process can attribute to the smaller defect sizes observed in the specimens fabricated from the re-used powder batch [9]. The decreased defect size in specimens fabricated from re-used powder results in them having longer fatigue lives as it takes longer time to develop stable cracks when pores are smaller.

The non-uniform packing state of unused powder was also verified by permeability results. The higher permeability of Batch 1 showed that the gas can flow easier through the powder due to less barriers and more empty spaces within the batch. The gas in these empty spaces may not completely escape the melt pool during melting and solidification in the AM process, and can be entrapped, introducing more gas-entrapped pores in the final fabricated parts. The reason for the smaller LoF defects, observed in the specimens fabricated from re-used powder compared with unused powder specimens (see Fig. 13(b) and Fig. 14(b)) is still unclear to authors. However, the thermal properties of the powder batches such as thermal conductivity may improve with re-using the powder [9] which may be attributed to the less compressibility and empty spaces of the re-used powder batch as compared to the unused one. Thus, the increase in thermal conductivity can lead to an increased energy absorption of the powder, resulting in a more stable melt pool and a better fusion between layers.

The difference in fatigue lives of the specimens from different locations can be illustrated based on the fact that powder is spread on the build plate using a recoater/wiper in the LB-PBF process. Therefore, some variations in powder characteristics in different locations can be expected as a result of spreading. These variations were also indicated by observing different types of defects on the fracture surface of machined specimens from the back compared with the counterparts from the front of the build plate. As seen in Fig. 13(b) and Fig. 14(b), the defects in specimens fabricated in the back were LoF, while in the specimens from the front, failure happened from gas-entrapped pores (see Fig. 13(a) and Fig. 14(a)). Additionally, the defect diameters (based on Murakami's approach [36]) of the specimens fabricated from Batch 1 and Batch 15 in the back were measured to be 90 μm and 69 μm, respectively, as compared to the counterparts in front with defect areas of 73 μm for Batch 1 and 34 μm for Batch 15. The smaller defect size in specimens fabricated in front compared to the ones fabricated in the back of the build plate (also see Fig. 7) explains the longer fatigue lives observed for specimens fabricated in front (see Fig. 11).

The observed difference between the defect distribution and size in the specimens from the same batch but fabricated in different locations can be attributed to the powder flowability. The presence of large agglomerates in the powder batch can disrupt the smooth flow of powder across the build plate by moving in lumps and leaving empty spots on the build plate [1,9]. Additionally, fine particles may deteriorate powder flowability due to higher interparticle frictions and cohesion between fine particles and their tendency to agglomeration [1,11,21,22,37–41]. Therefore, the unused powder with more very fine particles and large agglomerates had inferior flowability, resulting in poor powder spreadability and layer uniformity on the build plate. However, by continuously re-using the powder, the number of large agglomerates and fine particles decreased leaving particles with more comparable sizes in the re-used batch (see Fig. 3). Therefore, flowability improved by powder re-use resulting in less difference in fatigue lives of specimens from the re-used powder batch in different locations compared with specimens from unused powder, as evident from Figs. 11(a) and (b).

The improved flowability of the powder by re-using can be also understood by comparing the permeability and cohesion of different powder batches (see Fig. 5 and Fig. 6). Permeability decreased from Batch 1 to Batch 15 which can be related to the reduction of large agglomerates from the batch. In addition, powder cohesion, which evaluates the tendency of fine particles to agglomerate [1], decreased with powder re-use. Therefore, the combination of decreased permeability and lower cohesion can indicate that there are fewer fine particles as well as agglomerates within the re-used powder resulting in better flowability of this batch. It should be noted that the longer exposure of re-used powder to higher temperatures, and consequently, less moisture content, might have also contributed to some extent to the more flowability of re-used batch [1,12]. In the absence of humidity, re-used powder particles are less prone to agglomeration resulting in a more uniform powder layer on the build plate, and consequently, a smaller gap between the fatigue lives of front and back specimens in low, mid and high cycle fatigue regimes.

5. Conclusions

In this study, effects of powder re-use on mechanical properties of parts fabricated from 17−4 PH SS via LB-PBF additive manufacturing process were studied. In addition, the dependency of the mechanical properties on the location of the specimen on the build plate was also investigated. Specimens were fabricated and tested in two surface conditions; as-built and machined. The powder was continuously re-used in order to fabricate 15 consecutive sets. Powder characteristics were also analyzed in relation to the observed mechanical properties. Overall, the experimental results in this study have shown that both location of the specimen on the build plate and the powder characteristics, as they get affected by the powder re-use, can be influential on the fatigue performance of LB-PBF fabricated materials. In addition, based on the results, the following conclusions can be made:

1 The high cycle fatigue behavior of machined LB-PBF CA-H1025 17−4 PH SS specimens was observed to improve by continuously re-using the powder. Specimens fabricated from heavily re-used powder (re-used for 14-times) had a better fatigue strength in the high cycle regime than the specimens fabricated from unused powder.
2 The improved fatigue behavior in the high cycle regime was related to the reduced compressibility of the powder after re-use due to the reduction of agglomerates. Less agglomerates in the re-used batch reduces the presence of empty spaces in the powder bulk. This can result in smaller and less pores in the fabricated material.
3 Fatigue behavior of parts in the machined surface condition was observed to be dependent on the part location on the build plate with relatively higher fatigue lives for the specimens closer to the powder feed bin compared with the ones further away from the feed bin. However, the location dependency of the fatigue behavior was decreased with re-using the powder.
4 Powder flowability improved by continuously re-using the powder due to the reduction of fine particles and agglomerates in the re-used powder batches. This improved flowability was argued to be the main reason for the reduction in the location dependency of the fatigue behavior.
5 Fatigue behavior of parts in the as-built surface condition was insensitive to powder re-use or part location upon the build plate. Relatively high surface roughness as a result of the LB-PBF process

was the dominating factor affecting the fatigue degradation in both high and low cycle fatigue regimes.

6 No significant variation in tensile properties including yield and ultimate tensile strengths was observed as a result of powder re-use or specimen location on the build plate. Elongation to failure was observed to slightly increase by powder re-use and its effect on reducing the porosity.

In closing, the findings of this study indicate that powder characteristics can vary not only for successive builds but also for different locations on a single build; thus, highlighting the importance of standardizing powder handling and re-using/reconditioning practices. The existence of standardized practices can ensure repeatable quality builds across the build plate and on multiple platforms. Therefore, further studies are needed to better understand how each powder characteristic contributes to variations in defect formation and mechanical performance to be able to propose effective powder handling and re-use procedures/standards.

CRediT authorship contribution statement

Arash Soltani-Tehrani: Conceptualization, Methodology, Validation, Formal analysis, Data curation, Investigation, Writing - original draft, Visualization. **Jonathan Pegues:** Conceptualization, Methodology, Investigation, Formal analysis, Writing - original draft. **Nima Shamsaei:** Conceptualization, Methodology, Resources, Investigation, Writing - review & editing, Supervision, Project administration.

Declaration of Competing Interest

The authors declare that they have no known competing financial interests or personal relationships that could have appeared to influence the work reported in this paper.

Acknowledgements

This material is based upon work partially supported by the National Institute of Standards and Technology (NIST) under Award No.70NANB18H220. NASA MSFC is also acknowledged for performing the particle size distribution anlaysis. Jonathan Pegues is currently at the Sandia National Laboratories.

References

[1] J.H. Tan, W.L.E. Wong, K.W. Dalgarno, An overview of powder granulometry on feedstock and part performance in the selective laser melting process, Addit. Manuf. 18 (2017) 228–255, https://doi.org/10.1016/j.addma.2017.10.011.

[2] J.A. Slotwinski, E.J. Garboczi, P.E. Stutzman, C.F. Ferraris, S.S. Watson, M.A. Peltz, Characterization of metal powders used for additive manufacturing, J. Res. Inst. Stand. Technol. 119 (2014) 460–493, https://doi.org/10.6028/jres.119.018.

[3] J. Clayton, D. Millington-Smith, B. Armstrong, The application of powder rheology in additive manufacturing, JOM 67 (2015) 544–548, https://doi.org/10.1007/s11837-015-1293-z.

[4] L. Cordova, M. Campos, T. Tinga, Revealing the effects of powder reuse for selective laser melting by powder characterization, JOM (2019), https://doi.org/10.1007/s11837-018-3305-2.

[5] R. O'Leary, R. Setchi, P.W. Prickett, G. Hankins, N. Jones, An investigation into the recycling of Ti-6Al-4V powder used within SLM to improve sustainability, 2nd. Int. Conf. Sustain. Des. Manuf. 8 (2015) 377–388.

[6] P. Nandwana, W.H. Peter, R.R. Dehoff, L.E. Lowe, M.M. Kirka, F. Medina, et al., Recyclability study on inconel 718 and Ti-6Al-4V powders for use in Electron beam melting, Metall. Mater. Trans. B. 47 (2016) 754–762, https://doi.org/10.1007/s11663-015-0477-9.

[7] Y.Y. Sun, S. Gulizia, C.H. Oh, C. Doblin, Y.F. Yang, M. Qian, Manipulation and characterization of a novel titanium powder precursor for additive manufacturing applications, JOM 67 (2015) 564–572, https://doi.org/10.1007/s11837-015-1301-3.

[8] V. Seyda, N. Kaufmann, C. Emmelmann, Investigation of aging processes of Ti-6Al-4V powder material in laser melting, Phys. Procedia 39 (2012) 425–431, https://doi.org/10.1016/j.phpro.2012.10.057.

[9] P.E. Carrion, A. Soltani-Tehrani, N. Phan, N. Shamsaei, Powder recycling effects on the tensile and fatigue behavior of additively manufactured Ti-6Al-4V parts, JOM 71 (2019) 963–973, https://doi.org/10.1007/s11837-018-3248-7.

[10] P. Dastranjy Nezhadfar, A. Soltani-Tehrani, A. Sterling, N. Tsolas, N. Shamsaei, Effects of powder recycling on the mechanical properties of additively manufactured stainless steel 17-4PH, Solid Freeform Fabr. Symp. Proc. (2018) 1292–1300.

[11] A. Strondl, O. Lyckfeldt, H. Brodin, U. Ackelid, Characterization and control of powder properties for additive manufacturing, JOM 67 (2015) 549–554, https://doi.org/10.1007/s11837-015-1304-0.

[12] H.P. Tang, M. Qian, N. Liu, X.Z. Zhang, G.Y. Yang, J. Wang, Effect of powder reuse times on additive manufacturing of Ti-6Al-4V by selective Electron beam melting, JOM 67 (2015) 555–563, https://doi.org/10.1007/s11837-015-1300-4.

[13] L.C. Ardila, F. Garciandia, J.B. González-Díaz, P. Álvarez, A. Echeverria, M.M. Petite, et al., Effect of IN718 recycled powder reuse on properties of parts manufactured by means of Selective Laser Melting, Phys. Procedia 56 (2014) 99–107, https://doi.org/10.1016/j.phpro.2014.08.152.

[14] G. Jacob, C.U. Brown, M.A. Donmez, S.S. Watson, J. Slotwinski, Effects of powder recycling on stainless steel powder and built material properties in metal powder bed fusion processes, US Dep. Commer. Natl. Inst. Stand. Technol. (2017), https://doi.org/10.6028/NIST.AMS.100-6.

[15] P. Quinn, S. O'Halloran, J. Lawlor, R. Raghavendra, The effect of metal EOS 316L stainless steel additive manufacturing powder recycling on part characteristics and powder reusability, Adv. Mater. Process. Technol. 5 (2019) 348–359, https://doi.org/10.1080/2374068X.2019.1594602.

[16] B.A. Hann, Powder reuse and its effects on laser based powder fusion additive manufactured alloy 718, SAE Int. J. Aerosp. 9 (2016) 209–213, https://doi.org/10.4271/2016-01-2071.

[17] V.V. Popov, A. Katz-Demyanetz, A. Garkun, M. Bamberger, The effect of powder recycling on the mechanical properties and microstructure of Electron beam melted Ti-6Al-4 V specimens, Addit. Manuf. 22 (2018) 834–843, https://doi.org/10.1016/j.addma.2018.06.003.

[18] F. Ahmed, U. Ali, D. Sarker, E. Marzbanrad, K. Choi, Y. Mahmoodkhani, Study of powder recycling and its effect on printed parts during laser powder-bed fusion of 17-4 PH stainless steel, J. Mater. Process.Tech. (2019), https://doi.org/10.1016/j.jmatprotec.2019.116522.

[19] J. Pegues, M. Roach, R. Scott Williamson, N. Shamsaei, Surface roughness effects on the fatigue strength of additively manufactured Ti-6Al-4V, Int. J. Fatigue 116 (2018) 543–552, https://doi.org/10.1016/j.ijfatigue.2018.07.013.

[20] A. Yadollahi, N. Shamsaei, Additive manufacturing of fatigue resistant materials: challenges and opportunities, Int. J. Fatigue 98 (2017) 14–31, https://doi.org/10.1016/j.ijfatigue.2017.01.001.

[21] A.T. Sutton, C.S. Kriewall, M.C. Leu, J.W. Newkirk, Powder characterisation techniques and effects of powder characteristics on part properties in powder-bed fusion processes, Virtual Phys. Prototyp. 12 (2017) 3–29, https://doi.org/10.1080/17452759.2016.1250605.

[22] B. Liu, R. Wildman, C. Tuck, I. Ashcroft, R. Hague, Investigation the effect of particle size distribution on processing parameters optimisation in selective laser melting process, Int Solid Free Fabr Symp an Addit Manuf Conf (2011) 227–238, https://doi.org/10.1017/CBO9781107415324.004.

[23] G.K.H. Chua, C.Y.Y. Choong, C.H. Wong, Investigation of the effects on the print location during selective laser melting process, Proc. 3rd Int. Conf. Prog. Addit. Manufacuring (Pro-AM 2018) (2018) 613–618.

[24] M. Seifi, M. Gorelik, J. Waller, N. Hrabe, N. Shamsaei, S. Daniewicz, et al., Progress towards metal additive manufacturing standardization to support qualification and certification, JOM 69 (2017) 439–455, https://doi.org/10.1007/s11837-017-2265-2.

[25] R. Russell, D. Wells, J. Waller, B. Poorganji, E. Ott, T. Nakagawa, et al., Qualification and certification of metal additive manufactured hardware for aerospace applications, Addit. Manuf. Aerosp. Ind. (2019), https://doi.org/10.1016/b978-0-12-814062-8.00003-0.

[26] ASTM International, B215-15 Standard Practices for Sampling Metal Powders, ASTM Int, West Conshohocken, PA, 2015, https://doi.org/10.1520/B0215-15.

[27] ASTM International, E606/E606M-12 Standard Test Method for Strain-Controlled Fatigue Testing, ASTM Int, West Conshohocken, PA, 2012, https://doi.org/10.1520/E0606_E0606M-12.

[28] ASTM International, E8/E8M-13 Standard Test Methods for Tension Testing of Metallic Materials, ASTM Int, West Conshohocken, PA, 2013, https://doi.org/10.1520/E0008_E0008M-13.

[29] P.D. Nezhadfar, R. Shrestha, N. Phan, N. Shamsaei, Fatigue behavior of additively manufactured 17-4 PH stainless steel: synergistic effects of surface roughness and heat treatment, Int. J. Fatigue 124 (2019) 188–204, https://doi.org/10.1016/j.ijfatigue.2019.02.039.

[30] ASTM International, D7891-15 Standard Test Method for Shear Testing of Powders Using the Freeman Technology FT4 Powder Rheometer Shear Cell, ASTM Int, West Conshohocken, PA, 2015, https://doi.org/10.1520/D7891-15.

[31] ASTM International, E2651-19 Standard Guide for Powder Particle Size Analysis, ASTM Int, West Conshohocken, PA, 2019, https://doi.org/10.1520/E2651-19.

[32] X. Fu, D. Huck, L. Makein, B. Armstrong, U. Willen, T. Freeman, Effect of particle shape and size on flow properties of lactose powders, Particuology 10 (2012) 203–208, https://doi.org/10.1016/j.partic.2011.11.003.

[33] R. Freeman, Measuring the flow properties of consolidated, conditioned and aerated powders - A comparative study using a powder rheometer and a rotational shear cell, Powder Technol. 174 (2007) 25–33, https://doi.org/10.1016/j.powtec.2006.10.016.

[34] R.I. Stephens, A. Fatemi, R.I. Stephens, H.O. Fuchs, Metal Fatigue in Engineering, .

John Wiley & Sons, 2000.
[35] J.W. Pegues, N. Shamsaei, M.D. Roach, R.S. Williamson, Fatigue life estimation of additive manufactured parts in the as-built surface condition, Mater. Des. Process. Commun. (2019) e36, https://doi.org/10.1002/mdp2.36.
[36] Y. Murakami, Metal Fatigue- Effects of Small Defects and Nonmetallic Inclusions, (2002), https://doi.org/10.4293/108680811X13125733356710.
[37] C. Meier, R. Weissbach, J. Weinberg, W.A. Wall, A.J. Hart, Modeling and Characterization of Cohesion in Fine Metal Powders With a Focus on Additive Manufacturing Process Simulations, ArXiv Prepr ArXiv180406816 (2018), https://doi.org/10.1016/j.powtec.2018.11.072.
[38] I.E. Anderson, E.M.H. White, R. Dehoff, Feedstock powder processing research needs for additive manufacturing development, Curr. Opin. Solid State Mater. Sci. 22 (2018) 8–15, https://doi.org/10.1016/j.cossms.2018.01.002.
[39] C. Meier, R. Weissbach, J. Weinberg, W.A. Wall, A.J. Hart, Critical influences of particle size and adhesion on the powder layer uniformity in metal additive manufacturing, J. Mater. Process. Technol. 266 (2019) 484–501, https://doi.org/10.1016/j.jmatprotec.2018.10.037.
[40] J. Muñiz-Lerma, A. Nommeots-Nomm, K. Waters, M. Brochu, A comprehensive approach to powder feedstock characterization for powder bed fusion additive manufacturing: a case study on AlSi7Mg, Mater. Basel 11 (2018) 2386, https://doi.org/10.3390/ma11122386.
[41] A. Simchi, The role of particle size on the laser sintering of iron powder, Metall. Mater. Trans. B. 35 (2004) 937–948, https://doi.org/10.1007/s11663-004-0088-3.